POLITECNICO DI TORINO
Repository ISTITUZIONALE

Simulating the sintering of powder particles during the preheating step of Electron Beam Melting process: Review, challenges and a proposal

Original
Simulating the sintering of powder particles during the preheating step of Electron Beam Melting process: Review, challenges and a proposal / Rizza, G., Galati, M., Iuliano, L.. - 112:(2022), pp. 388-393. (15th CIRP Conference on Intelligent Computation in Manufacturing Engineering, ICME 2021 Gulf of Naples, Italy 14-16 July 2021) [10.1016/j.procir.2022.09.025].

Availability:
This version is available at: 11583/2973996 since: 2022-12-20T13:27:46Z

Publisher:
Elsevier B.V.

Published
DOI:10.1016/j.procir.2022.09.025

Terms of use:

This article is made available under terms and conditions as specified in the corresponding bibliographic description in the repository

Publisher copyright

(Article begins on next page)

28 November 2026

Available online at www.sciencedirect.com

ScienceDirect

Procedia CIRP 112 (2022) 388–393

www.elsevier.com/locate/procedia

15th CIRP Conference on Intelligent Computation in Manufacturing Engineering, Gulf of Naples, Italy

Simulating the sintering of powder particles during the preheating step of Electron Beam Melting process: review, challenges and a proposal

Giovanni Rizza[a]*, Manuela Galati[a], Luca Iuliano[a]

[a]*Department od Management and Production Engineering (DIGEP), Integrated Additive Manufacturing center (IAM@PoliTo), Politecnico di Torino, Corso Duca degli Abruzzi 24, 10129 Torino, Italy*

* *Corresponding author. Tel.: +39 0110907280.* E-mail address: *giovanni.rizza@polito.it*

Abstract

The powder bed preheating before melting is a distinctive manufacturing step of the Electron Beam Melting (EBM) process. During preheating slight sintering occurs and small necks are formed between neighbouring particles. The necks improve the heat transfer and the powder bed strength allowing a reduction of supports structures and the neutralisation of the so-called smoke. However, preheating may represent over 50% of the total production time. This work investigates the major strategies in literature for preheating phase optimisation and proposes a numerical simulation approach to evaluate the neck growth and the corresponding sintering level.

© 2022 The Authors. Published by Elsevier B.V.
This is an open access article under the CC BY-NC-ND license (https://creativecommons.org/licenses/by-nc-nd/4.0)
Peer-review under responsibility of the scientific committee of the 15th CIRP Conference on Intelligent Computation in Manufacturing Engineering, 14-16 July, Gulf of Naples, Italy

Keywords: Additive Manufacturing; Temperature; Phase-field; Sintering degree; Process optimisation.

1. Introduction

Preheating is a characteristic step that distinguishes Electron Beam Melting (EBM) from other metal Additive Manufacturing (AM) techniques [1]. This step precedes the melting phase and aims to partially sinter the powder bed. During the sintering phase, small necks are formed between adjacent powder particles [2]. The sintering degree needs to be precisely controlled to prevent pushing phenomena, also known as “smoke” [3]. This effect may be generated by the accumulation of negative electrostatic charges [4] or the momentum transferred by the electrons greater than the weight of powder particles [5]. The sintering increases the apparent weight of powder bed particles and the electric conductivity, allowing a better dispersion of negative charges. The sintering increases also the thermal conductivity of the powder bed [2], which is beneficial to keep a uniform temperature, avoid high thermal gradient between the melt pool and the surrounding and allow a faster dissipation of thermal energy generated during the melting of overhanging structures [6]. The preheating of the powder bed before the melting, together with the initial heating of the build platform before starting the whole process and the vacuum environment [1], create the hot working environment that characterises the EBM process. Both the build platform and the powder bed heating aim to achieve gradually a specific temperature, that is related to the material processed.

The effective production begins after achieving the right chamber pressure (10^{-3} Pa [7]) and the build platform temperature [8]. For each layer and until the entire part is completed, a layer of powder is distributed on the build platform by a rake system and it is preheated by a series of passages of a defocused electron beam at high current and speed [1] in two steps: preheating one and preheating two with the aims above mentioned. During preheating one, the electron beam scans an area corresponding to the maximum rectangular area which includes all the components. During preheating two, the preheating takes place in a smaller area corresponding to an offset of the section to be melted [9]. After melting, a further post-heating step may take place using the same

2212-8271 © 2022 The Authors. Published by Elsevier B.V.
This is an open access article under the CC BY-NC-ND license (https://creativecommons.org/licenses/by-nc-nd/4.0)
Peer-review under responsibility of the scientific committee of the 15th CIRP Conference on Intelligent Computation in Manufacturing Engineering, 14-16 July, Gulf of Naples, Italy
10.1016/j.procir.2022.09.025

parameters of preheating two on the same area of preheating one. Each production step is controlled by a specific set of parameters, that are fine-tuned according to the material and the powder characteristics. As regard preheating, the sintering degree of the powder is defined by the following main process parameters: the beam speed, the beam current, the number of scan repetitions and the distance between adjacent scanned lines [10]. In particular, keeping constant the other process parameters, the scan repetitions establish the powder bed temperature and therefore the sintering degree. The process setting is identified empirically by performing a single job without melted parts in which the preheating parameters are initially adjusted until no smoke phenomenon occurs when the electrons hit the powder particles. Then, the parameters are changed to produce a certain level of sintering. At the end of this job, a technician evaluates the sintering degree observing the strength of the powder bed. Since, often, the time to preheat the powder is much longer than the melting, also the time required to perform the preheating step is kept under consideration during the optimisation. The preheating parameters are set therefore as trade-off between a specific degree of sintering which is achieved in the shortest time possible.

Since the empirical nature of this approach, the procedure is time-consuming, expensive and the results are strictly related to the technician capabilities to judge the quality of the preheating. Because of that often, further optimizations of this phase are required during the real job to increase the level of sintering or to reduce the time to perform the preheating of the layer. Despite this tuning operation, often the time to perform the preheating plus the post-heating phase is ten times longer than the melting phase.

A numerical simulation is a powerful tool for optimizing the production process and identify the so-called production window [11]. The use of numerical simulation allows the reduction of uncertainty margins and the costs related to the process development. In the case of complex processes, such as EBM, process simulation could also help to better understand the physical phenomena that occur, since the difficulty to access the build chamber during the process and acquire productions data with external sensors [12]. The power of this approach is demonstrated by a large number of models at different scales and accuracy levels [13] available in the literature to simulate the melting phase of the EBM process. Most of the models assumed the preheated powder bed as a continuum. Material properties of the powder such as the density, thermal conductivity or specific heat are modelled as dependent on corresponding bulk material linearly [14] or non-linearly [12,13,15,16]. Other studies attempted to analyze the material properties experimentally by producing samples of sintered powder [17,18]. Leung et al. [17] produced cylindrical specimens that contain sintered powder particles and scanned the samples with X-ray computed tomography, to evaluate the degree of sintering and the properties of the sintered powder. Gong and Chou [18] analysed a sample of sintered powder taken from an edge of the powder cake and a sample of powder contained in a hollowed cylinder. A stereomicroscope was adopted to characterise the degree of sintering. However, for both studies, the results are strictly related to the specific material and process conditions. The model proposed by Körner et al. [19] overcame the issues associated with the powder properties, considered a powder-to-powder modelling approach. The preheating step and its effect on the powder bed before the melting step were neglected. Overall, the simulation models remain centred on the melting step only. Despite the preheating step and its effect on powder particles are the base of the EBM process, that aspect lacks investigation and reliable methods are still required.

This work provides an overview of the current state of the art of sintering and preheating simulations. A modification of the traditional approach is presented to provide a viable alternative to simulate the sintering phenomenon that occurs during the preheating step of the EBM process. A comparison between the conventional and the proposed models is shown.

2. Literature review

Sintering is an ancient technique empirically adopted to process ceramic materials and metals. During sintering, particles bond together by mass transport mechanisms at an atomic scale forming solid objects [20]. Atom diffusion is activated by thermal energy and driven by a reduction of the free energy of the system [21]. The temperature, the pressure, the size and the shape of the particles, the atmosphere and the chemical composition are the main parameters that influence the sintering. According to these factors, different diffusion mechanisms can act. Volume diffusion from different sources (D_V), grain boundary diffusion (D_{GB}), viscous flow (η), surface diffusion (D_s) and vapour diffusion (D_{Vap}) [22] are the principal diffusion mechanisms. Fig. 1 depicts the diffusion mechanisms and the respective source of atoms. The neck radius (X) and the particle diameter (D) are also showed. These diffusion mechanisms at the base of the traditional sintering are also equivalent to the ones during the preheating phase. The significant difference is the scope of the sintering. While the objective of traditional sintering is to obtain a high-density component with a high sintering rate, in EBM, the sintering aims only to give the proper stability to the powder bed [10]. Because of that, in the traditional manufacturing processes such as powder metallurgy, pressure is applied to compact the powder particles and the sintering process may require hours to achieve the desired degree of density[23].

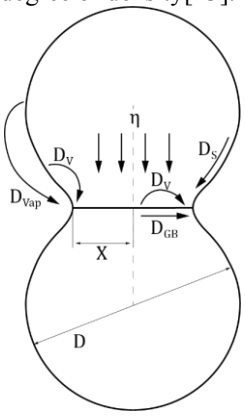


Fig. 1. Diffusion mechanisms, with respective atom source and the main geometric dimensions. X is the neck radius and D is the particle diameter.

Historically, most of the research about sintering has been focused on the experimental investigation on the final density and hardness of the obtained product [24,25]. Only between 1945 to 1955, the research on sinter modelling became more structured [25]. Frenkel [26] proposed the first mathematical model, in which the sintering was investigated as a viscous flow that leads to a progressive bond between the powder particles. With some modifications and despite the diffusion or plastic flow and the influence of grain boundaries were neglected, this model is still currently adopted for the description of the neck growth. Kuczynski [27] proposed a mathematical model based on the viscous flow considering also surface diffusion and a mechanism similar to volume diffusion. However, even in this case, the grain boundary was neglected and the densification was not well described. These preliminary models were followed by quantitative models that investigated the influence of sintering conditions on the shrinkage and density of sintered components [28,29]. Kingery and Berg [30] developed a model for solid-state sintering that described also the influence of the particle size and the grain boundary and were able to converge the shrinkage phenomena to diffusion phenomena during sintering. Based on these models, during the seventies, new simulation approaches were developed [31] to account for more complex particles geometries and the coexistence of different diffusion mechanisms [22,32–34]. The idea to perform computer simulation of sintering arose in 1965 with the work by Nichols and Mullins [35]. In that work, numerical simulations were performed for the sintering of spherical particles under surface diffusion mechanisms, while neglecting the grain boundaries.

Today, the most adopted approaches to perform sintering simulations are Monte Carlo simulations and finite element (FE) modelling. While the first analyses different what-if scenarios [36] by a stochastic approach, the FE method considers the densification of powder particles under the effect of specific boundary conditions [37]. Because of the rather simple modelling, both approaches fail to correlate the influence of microstructural and diffusion characteristics on the consolidation mechanisms during the sintering of three-dimensional powder particles. Additionally, those approaches cannot account for different complex diffusion mechanisms simultaneously [37]. An alternative numerical technique is phase-field modelling [38], in which is possible to consider the complex phenomena that contribute to the material densification and particles movement. Phase-field modelling was used for many application fields such as the simulation of the diffusion [39], the solidification [40], the solid-state phase transformation [41], the grain growth [42], the translation of defects [43], crack propagation [44] and other applications [37]. The most relevant advantage of the phase-field approach is the description of the arbitrary microstructure evolution, without tracking the interface position or imposing any particular boundary condition [37].

In phase-field models, the microstructural characteristics, both structural/compositional and the interface, are identified as phase-field variables [37]. These variables refer to specific physic parameters and assume well-defined values inside the boundaries of each particle. These values can change rapidly but smoothly along the boundaries of the particles or grains [37]. This characteristic is fundamental, as the interface of the particles is automatically described by the evolution of phase-field variables [37]. The field variables can be distinguished in conserved and non-conserved. Conserved variables contain information about the local composition and describe characteristics as density or molar fraction [45]. Non-conserved variables represent information about local structure and orientation. These variables may be used to distinguish among coexisting phases with different characteristics, or different grains or particles [45,46]. Changes in both conserved and non-conserved variables involve changes in the microstructure and properties of the considered system [37]. What drives the evolution in space and time of the variables is the reduction of the free energy of the system [37], which is built as a functional of the conserved and non-conserved variables.

As regards the sintering which occurs during the EBM process, to the best of the authors' knowledge, only one study has been performed [47]. The temperature applied to determine the sintering degree has been considered constant and the processing parameters and grain structure appeared insignificant. However, as above mentioned the temperature increases gradually first during the powder spreading and then by the subsequent beam passages during the preheating one and two. The effective sintering process during EBM and therefore the effect of the gradual increase of the temperature on the particles has been never considered in the literature.

3. Methodology

Since the power of the phase-field modelling in simulating the conventional sintering process, in this work, this approach is adopted and adapted to simulate the sintering phenomena that occur during the EBM process.

In the phase-field method, the evolution of microstructure is given by the minimization of system free energy, expressed as:

$$F = \int \left[f(c,\eta_i) + \frac{1}{2} k_c |\nabla c|^2 + \frac{1}{2} \sum_i k_{\eta_i} |\nabla \eta_i|^2 \right] dV \qquad (1)$$

The term $f(c,\eta_i)$ represents the bulk contribution of the free energy of the system, while the second and the third terms represent the excess of interfacial energy at the interface of the particle/void phase and the grain boundaries respectively [48]. Equation (1) is a function of the phase-field variables c and η_i. c is the conserved field representing the concentration. It assumes a value of 1 inside the material and 0 outside the material. For this model, c was considered as the density of the material. η_i represents the non conserved field that describes the morphological evolution of the powder particles. It assumes a value of 1 inside the i^{th} particle and 0 elsewhere inside the simulation domain.

The bulk contribution of the free energy was expressed in terms of phase-field variables according to Ref. [48]:

$$f(c,\eta_i) = Ac^2(1-c)^2 + B\left[c^2 + 6(1-c)\sum_i \eta_i^2 - 4(2-c)\sum_i \eta_i^3 + 3\left(\sum_i \eta_i^2\right)^2\right] \qquad (3)$$

A and B are coefficients strictly related to the material properties and were evaluated as:

$$A = \frac{(12\gamma_s - 7\gamma_{GB_{ij}})}{\delta} \quad (4)$$

$$B = \frac{\gamma_{GB_{ij}}}{\delta} \quad (5)$$

γ_s and $\gamma_{GB_{ij}}$ represent the surface energy of the particles and the grain boundary energy among the i^{th} and j^{th} particle, respectively. δ is the interface width, which was assumed equal to the grain boundary thickness. The gradient coefficients were calculated as follows:

$$k_c = \frac{3}{4}\delta\left(2\gamma_s - \gamma_{GB_{ij}}\right) \quad (6)$$

$$k_{\eta_i} = \frac{3}{4}\left(\delta\gamma_{GB_{ij}}\right) \quad (7)$$

The spatial and time evolution of the phase-field variables was described by different equations for the conserved variables and the non-conserved variables. Cahn-Hilliard (CH) equation has been used to describe the behavior of conserved variables, according to Ref. [49]:

$$\frac{\partial c}{\partial t} = \nabla\left(\widehat{M}\nabla\frac{\delta F}{\delta c(x,t)}\right) = \nabla\left(M\nabla\left(\frac{\partial f}{\partial c} - k_c\nabla^2 c\right)\right) \quad (8)$$

Where $\widehat{M}$ is the concentration mobility tensor, x is the spatial position vector and t is the simulation time. The concentration mobility tensor was defined as:

$$\widehat{M} = \frac{\widehat{D}\Omega}{k_b T} \quad (9)$$

Where Ω is the molar volume, k_B is the Boltzmann constant and T is the temperature. $\widehat{D}$ is the diffusivity tensors and was described in Equation (10), according to Ref. [48]:

$$\widehat{D} = D_{vol}\phi_b(c)\hat{I} + D_{surf}\phi_s(c)\hat{T}_s + D_{GB}\sum_i\sum_j \eta_i\eta_j\,\hat{T}_{GB_{ij}} \quad (10)$$

Where $\hat{I}$ represents the identity matrix; $\phi_b(c)$ and $\phi_s(c)$ are the interpolation functions, adopted to activate each diffusion mechanism in the corresponding area of interest and expressed by Equations (11) and (12); The three terms D_{vol}, D_{surf} and D_{GB} represent the volume, the surface and the grain boundary diffusion coefficients, respectively, and were calculated according to an Arrhenius-type equation such as Equation (13), in which D^0 represent a constant specific for each diffusion mechanism and Q is the activation energy of that diffusion phenomena. Both values are strictly related to the simulated material. k_B is the Boltzmann constant while T is the absolute temperature. $\hat{T}_s$ and $\hat{T}_{GB_{ij}}$ are the projection tensors that specify the direction of surface and grain boundary diffusion, respectively. These tensors were calculated as gradients of the phase-field variables as expressed in Equations (14) and (15), where $\overrightarrow{n_s}$ represents the unit vector normal to the interface between the particle and the void phase; $\vec{n}_{GB_{ij}}$represents the unit vector normal to grain boundary between the i^{th} particle and the j^{th} particle.

$$\phi_b(c) = c^3(10 - 15c + 6c^2) \quad (11)$$

$$\phi_s(c) = 30c^2(1-c)^2 \quad (12)$$

$$D = D^0 e^{\left(-\frac{Q}{k_B T}\right)} \quad (13)$$

$$\hat{T}_s = \hat{I} - \overrightarrow{n_s}\otimes\overrightarrow{n_s} \text{ with } \overrightarrow{n_s} = \frac{\nabla c}{|\nabla c|} \quad (14)$$

$$\hat{T}_{GB_{ij}} = \hat{I} - \vec{n}_{GB_{ij}}\otimes\vec{n}_{GB_{ij}} \text{ with } \vec{n}_{GB_{ij}} = \frac{\nabla\eta_i - \nabla\eta_j}{|\nabla\eta_i - \nabla\eta_j|} \quad (15)$$

The non-conserved variables evolve following the Allen-Cahn (AC) equation according to Ref. [49]:

$$\frac{\partial\eta_i}{\partial t} = -L\left(\frac{\delta F}{\delta\eta_i}\right) = -L\left(\frac{\delta f(c,\eta_i)}{\delta\eta_i} - k_{\eta_i}\nabla^2\eta_i\right) \quad (16)$$

where L is the order parameter scalar mobility and was defined as expressed in Equation (17) in which ϑ_{GB} is the grain boundary mobility

$$L = \frac{\vartheta_{GB}\gamma_{GB}}{\kappa_{\eta_i}} \quad (17)$$

The phase-field model described by Equation (8) and Equation (16) was implemented in the Multiphysics Object-Oriented Simulation Environment (MOOSE) [50] developed at Idaho National Lab. Equation (8) is a fourth-order differential equation and was divided into two differential equations of second order by introducing an additional phase field variable called μ, obtaining Equation (18) and Equation (19).

$$\frac{\partial c}{\partial t} = \frac{\partial}{\partial x_i}\left(M_{ij}\frac{\partial\mu}{\partial x_j}\right) \quad (18)$$

$$\mu = \frac{\partial f}{\partial c} - \kappa_c\nabla^2 c \quad (19)$$

Partial differential equations were implemented in the weak form. For Equations (16), (18) and (19) the weak form was derived by Ref. [37]:

$$\left(\frac{\partial c}{\partial t},\psi_m\right) = (M\nabla\mu,\nabla\psi_m) - \langle M\nabla\mu.\vec{n},\psi_m\rangle \quad (20)$$

$$(\mu,\psi_m) = \left(\frac{\partial f}{\partial c},\psi_m\right) + (k_c\nabla c,\nabla\psi_m) - \langle k_c\nabla c.\vec{n},\psi_m\rangle \quad (21)$$

$$\left(\frac{\partial\eta_i}{\partial t},\psi_m\right) = -L\left(\frac{\partial f}{\partial c},\psi_m\right) + L\left(k_{\eta_i}\nabla\eta_i,\nabla\psi_m\right) - L\left(k_{\eta_i}\nabla\eta_i.\vec{n},\psi_m\right) \quad (22)$$

Where $\psi_m$is a test function, (.) denotes a volume integration and $\langle . \rangle$ denotes a boundary integration. Further details about the mathematical model and the numerical scheme to solve these equations can be found Ref. [51].

As can be observed, Equations (9) and (13) depend on the current sintering temperature and therefore need to be evaluated at each simulation step and updated automatically according to the temperature value at the corresponding simulation step.

4. Model validation

The implemented model has been validated considering the studies by Chockalingam et al. [49] and Asoro et al. [52]. To replicate the simulation conditions [49] and the experimental one [52], the sintering of two equal spherical silver particles with a diameter of 40 nm was performed at a temperature equal to 673.15 K, for 900 s. A simulation domain of 100 nm x 50 nm was considered. A mesh size of 0.5 nm and nine-node quadratic elements were adopted. To improve the efficiency of the simulation, time step and mesh adaptivity mechanisms were used while superimposing a maximum step size of 1 s to avoid simulation instabilities. According to Ref. [49], the rigid body motion was not considered and only surface, grain boundary and bulk diffusion mechanism were included. Grain boundary diffusion was considered equal to $0.1D_s$. The interface width was set to 2 nm and the material properties were extracted by Chockalingam et al. [49]

The material properties and the modelling parameters were converted in non-dimensional quantities adopting a length scale coefficient equal to $1x10^{-9}$ m, a time scale coefficient of $1x10^{-3}$ s and an energy coefficient equal to 1 eV.

The simulation was performed on a desktop computer (Intel® Core ™ i5-7500 @3.40 GHz and 16 GB of RAM) and required about 25 hours.

Fig. 2 reports the comparison at t=0 s, t=180 s and t=900s between the experimental results obtained by Asoro et al. [52], the simulation results obtained by Chockalingam et al. [49] and the simulation results obtained by the presented model. To compare the simulation results, the concentration field was considered. The simulation results were in good agreement with Chockalingam et al. [49], while the experiments showed a different dihedral angle. This deviation was already pointed out by Chockalingam et al. and attributed to the ratio between γ_s and γ_{GB} , which is strongly dependent on the dihedral angle ϕ as follows:

$$\gamma_s = 2\gamma_{GB}\cos\left(\frac{\phi}{2}\right) \quad (23)$$

However, slight changes in surface energy or in the grain boundary energy or the presence of impurities may also produce different dihedral angles. Another possible cause of this difference may be the rigid body motion mechanism of the powder particles, which has been neglected in the simulation.

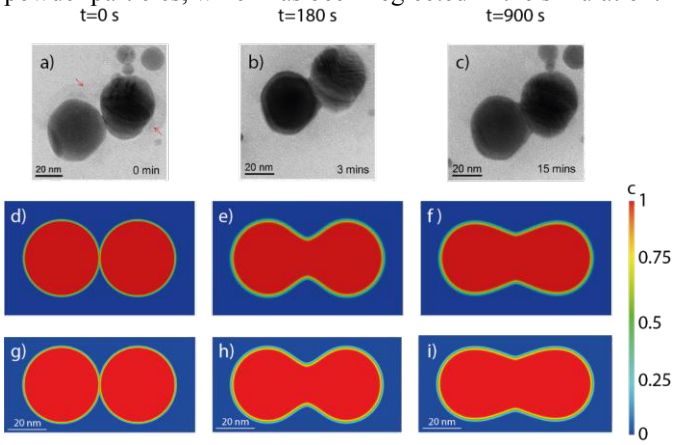


Fig. 2. Results of sintering simulation at a constant temperature. From a) to c): experimental images of sintering of silver nanoparticles (reprinted from [52] with permission from Elsevier). From d) to f): phase-field simulation of sintering of silver nanoparticles (reprinted from [49] with the permission from Elsevier). From g) to i) represent the phase-field simulation of sintering with the model presented in the current work.

5. Effect of the application of a variable temperature field during the sintering

As above mentioned, the condition of a constant temperature over a certain time is not well representative of the sintering conditions during the EBM process. In fact, the EBM process is not a steady-state process. To investigate the different neck growth generated by the application of a linear temperature profile with respect to a steady temperature, the simulation presented in the paragraph above was repeated using the proposed approach. The temperature load was increased gradually from 570.15 K to 673.15 K, from 0 to 180 s, respectively. The initial temperature is lower than the final to better mimic the process conditions during the preheating phase of the EBM process. The simulation was performed for 180 s. To achieve the maximum temperature, this has been increased of 24.6 K each 30s (Fig. 4), while the other variables have been kept equal to the model used for the validation.

Fig. 3 reports the comparison between the shape and the size of the neck after 180 s using the constant temperature and linear profile. The first evidence is that the resulting shape of the neck is significantly different.

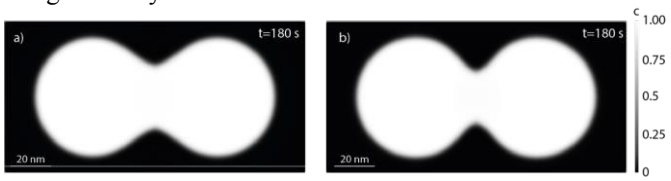


Fig. 3. a) concentration field of the simulation at constant temperature; b) concentration field of the simulation at growing temperature.

Fig. 4 compares the neck growth over time for the simulation carried out at variable and constant temperature. In the case of variable temperature for each temperature increment, there is a trend change in the growth rate of the neck. In the case of variable temperature, the neck radius is always smaller values than the corresponding time at a constant temperature. This result highlights the strong influence of the temperature profile on the sintering degree and confirms the observation presented in Fig. 3 for the concentration field.

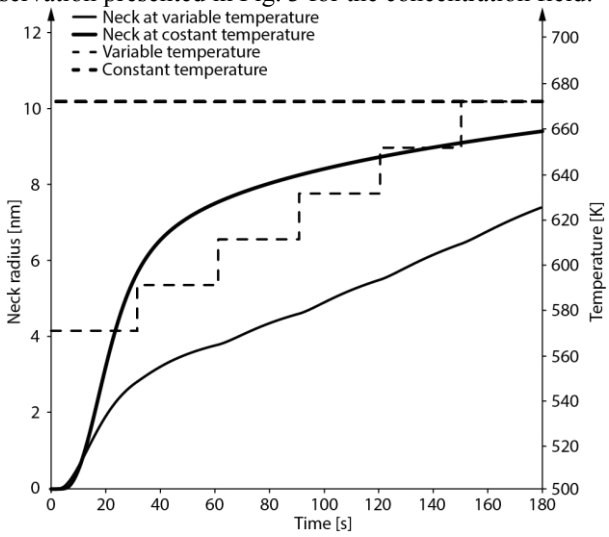


Fig. 4. Evolution of the neck radius at a constant temperature, at a variable temperature and evolution of the temperature with sintering time

6. Conclusions

The preheating step is fundamental for the EBM process. The definition of good process parameters for this process step is a time consuming and economically expensive operation. A phase-field model was proposed as a numerical approach capable to perform the simulation of preheating step. The model has proven the capabilities to simulate traditional sintering, conducted at a constant temperature. However, to simulate the preheating for EBM, the sintering under increasing temperature has been simulated. The results showed that the temperature history has an high influence on the resulting neck dimension and therefore on the sintering degree. This result disproves the application of traditional sintering models for the sintering that occurs during the EBM preheating and represents

an initial footstep in the simulation of the sintering phenomena during preheating.

References

[1] Galati M, Rizza G, Defanti S, Denti L. Surface roughness prediction model for Electron Beam Melting (EBM) processing Ti6Al4V. Precis. Eng. 2021; 19–28.

[2] Cheng B, Chou K. Thermal stresses associated with part overhang geometry in electron beam additive manufacturing: process parameter effects, in: Proc. Annu. Int. Solid Free. Fabr. Symp, 2014: p. 1076.

[3] Minetola P, Galati M. A challenge for enhancing the dimensional accuracy of a low-cost 3D printer by means of self-replicated parts. Addit. Manuf. 2018;

[4] Sigl M, Lutzmann S, Zäh MF. Transient physical effects in electron beam sintering, in: 2006 Int. Solid Free. Fabr. Symp., 2006.

[5] Qi HB, Yan YN, Lin F, He W, Zhang RJ. Direct metal part forming of 316L stainless steel powder by electron beam selective melting. Proc. Inst. Mech. Eng. Part B-Journal Eng. Manuf. 2006; 1845–1853.

[6] Smith CJ, Tammas-Williams S, Hernandez-Nava E, Todd I. Tailoring the thermal conductivity of the powder bed in Electron Beam Melting (EBM) Additive Manufacturing. Sci. Rep. 2017; 1–8.

[7] Galati M, Iuliano L. A literature review of powder-based electron beam melting focusing on numerical simulations. Addit. Manuf. 2018; 1–20.

[8] Lunetto V, Galati M, Settineri L, Iuliano L. Unit process energy consumption analysis and models for Electron Beam Melting (EBM): Effects of process and part designs. Addit. Manuf. 2020; 101115.

[9] Körner C. Additive manufacturing of metallic components by selective electron beam melting—a review. Int. Mater. Rev. 2016; 1–17.

[10] Larsson M, Snis A. Method and device for producing three-dimensional objects, 06758093.6, 2008.

[11] Galati M, Snis A, Iuliano L. Powder bed properties modelling and 3D thermo-mechanical simulation of the additive manufacturing Electron Beam Melting process. Addit. Manuf. 2019;

[12] Cheng B, Price S, Lydon J, Cooper K, Chou K. On Process Temperature in Powder-Bed Electron Beam Additive Manufacturing: Model Development and Validation. J. Manuf. Sci. Eng. Asme. 2014; 1–12.

[13] Galati M, Iuliano L, Salmi A, Atzeni E. Modelling energy source and powder properties for the development of a thermal FE model of the EBM additive manufacturing process. Addit. Manuf. 2017; 49–59.

[14] Qi HB, Yan YN, Lin F, Zhang RJ. Scanning method of filling lines in electron beam selective melting. Proc. Inst. Mech. Eng. Part B J. Eng. Manuf. 2007; 1685–1694.

[15] Zäh MF, Lutzmann S. Modelling and simulation of electron beam melting. Prod. Eng. 2010; 15–23.

[16] Shen N, Chou K. Numerical thermal analysis in electron beam additive manufacturing with preheating effects, in: 23rd Annu. Int. Solid Free. Fabr. Symp. - An Addit. Manuf. Conf. SFF 2012, 2012: pp. 774–784.

[17] Leung CLA, Tosi R, Muzangaza E, Nonni S, Withers PJ, Lee PD. Effect of preheating on the thermal, microstructural and mechanical properties of selective electron beam melted Ti-6Al-4V components. Mater. Des. 2019; 107792.

[18] Gong X, Chou K. Characterization of sintered TI-6AL-4V powders in electron beam additive manufacturing, in: ASME 2013 Int. Manuf. Sci. Eng. Conf. Collocated with 41st North Am. Manuf. Res. Conf. MSEC 2013, American Society of Mechanical Engineers Digital Collection, 2013.

[19] Körner C, Attar E, Heinl P, Korner C, Attar E, Heinl P. Mesoscopic simulation of selective beam melting processes. J. Mater. Process. Technol. 2011; 978–987.

[20] German R. Sintering: From Empirical Observations to Scientific Principles, Elsevier Inc., 2014.

[21] Kang SJ. Sintering, Elsevier Ltd, 2005.

[22] Ashby MF. A first report on sintering diagrams. Acta Metall. 1974; 275–289.

[23] Torres Y, Pavo´n JJ, Pavo´n P, Nieto I, Rodri´guez JA, Rodri´guez R. Conventional Powder Metallurgy Process and Characterization of Porous Titanium for Biomedical Applications. n.d.;

[24] Biswas S, Schwen D, Tomar V. Implementation of a phase field model for simulating evolution of two powder particles representing microstructural changes during sintering. J. Mater. Sci. 2018; 5799–5825.

[25] German RM. The Emergence of Quantitative Sintering Theory from 1945 to 1955. JOM. 2017; 630–634.

[26] FRENKEL, J. J. Viscous flow of crystalline bodies under the action of surface tension. J. Phys. 1945; 385.

[27] Kuczynski GC. Self-diffusion in sintering of metallic particles. JOM. 1949; 169–178.

[28] Allison EB, Murray P. A fundamental investigation of the mechanism of sintering. Acta Metall. 1954; 487–512.

[29] Rhines FN, Cannon HS. Rate of Sintering of Copper Under a Dead Load. JOM. 1951; 529–530.

[30] Kingery WD, Berg M. Study of the initial stages of sintering solids by viscous flow, evaporation-condensation, and self-diffusion. J. Appl. Phys. 1955; 1205–1212.

[31] Kraft T, Riedel H. Numerical simulation of solid state sintering; model and application. J. Eur. Ceram. Soc. 2004; 345–361.

[32] Johnson DL. New method of obtaining volume, grain-boundary, and surface diffusion coefficients from sintering data. J. Appl. Phys. 1969; 192–200.

[33] Beere W. The second stage sintering kinetics of powder compacts. Acta Metall. 1975; 139–145.

[34] Bross P, Exner HE. Computer simulation of sintering processes. Acta Metall. 1979; 1013–1020.

[35] Nichols FA, Mullins WW. Morphological changes of a surface of revolution due to capillarity-induced surface diffusion. J. Appl. Phys. 1965; 1826–1835.

[36] Tikare V, Braginsky M, Olevsky EA. Numerical simulation of solid-state sintering: I, sintering of three particles. J. Am. Ceram. Soc. 2003; 49–53.

[37] Biswas S, Schwen D, Singh J, Tomar V. A study of the evolution of microstructure and consolidation kinetics during sintering using a phase field modeling based approach. Extrem. Mech. Lett. 2016; 78–89.

[38] Wang YU. Computer modeling and simulation of solid-state sintering: A phase field approach. Acta Mater. 2006; 953–961.

[39] Hu SY, Henager CH. Phase-field simulation of void migration in a temperature gradient. Acta Mater. 2010; 3230–3237.

[40] Loginova I, Amberg G, Ågren J. Phase-field simulations of non-isothermal binary alloy solidification. Acta Mater. 2001; 573–581.

[41] Jin YM, Artemev A, Khachaturyan AG. Three-dimensional phase field model of low-symmetry martensitic transformation in polycrystal: Simulation of ζ'2 martensite in AuCd alloys. Acta Mater. 2001; 2309–2320.

[42] Uehara T, Tsujino T, Ohno N. Elasto-plastic simulation of stress evolution during grain growth using a phase field model. J. Cryst. Growth. 2007; 530–537.

[43] Hu SY, Baskes MI, Stan M. Phase-field modeling of microvoid evolution under elastic-plastic deformation. Appl. Phys. Lett. 2007; 081921.

[44] Karma A, Kessler DA, Levine H. Phase-field model of mode III dynamic fracture. Phys. Rev. Lett. 2001; 45501-1-45501–4.

[45] Moelans N, Blanpain B, Wollants P. An introduction to phase-field modeling of microstructure evolution. Calphad Comput. Coupling Phase Diagrams Thermochem. 2008; 268–294.

[46] Deng J. A Phase Field Model of Sintering with Direction-Dependent Diffusion. 2012;

[47] Yan W, Ma W, Shen Y. Powder sintering mechanisms during the pre-heating procedure of electron beam additive manufacturing. Mater. Today Commun. 2020; 101579.

[48] Biswas S, Schwen D, Wang H, Okuniewski M, Tomar V. Phase field modeling of sintering: Role of grain orientation and anisotropic properties. Comput. Mater. Sci. 2018; 307–319.

[49] Chockalingam K, Kouznetsova VG, van der Sluis O, Geers MGD. 2D Phase field modeling of sintering of silver nanoparticles. Comput. Methods Appl. Mech. Eng. 2016; 492–508.

[50] Permann CJ, Gaston DR, Andrš D, Carlsen RW, Kong F, Lindsay AD, Miller JM, Peterson JW, Slaughter AE, Stogner RH, Martineau RC. MOOSE: Enabling massively parallel multiphysics simulation. SoftwareX. 2020; 100430.

[51] Tonks MR, Gaston D, Millett PC, Andrs D, Talbot P. An object-oriented finite element framework for multiphysics phase field simulations. Comput. Mater. Sci. 2012; 20–29.

[52] Asoro MA, Ferreira PJ, Kovar D. In situ transmission electron microscopy and scanning transmission electron microscopy studies of sintering of Ag and Pt nanoparticles. Acta Mater. 2014; 173–183.